

Supplementary Information for
**“Synthesis, Characterization, and Growth Mechanism of Motifs
of Ultrathin Cobalt-substituted NaFeSi₂O₆ Nanowires”**

Crystal S. Lewis¹, Dominic Moronta¹, Maxwell W. Terban², Lei Wang¹, Shiyu Yue¹,
Cheng Zhang³, Qiang Li³, Adam Corrao¹, Simon J. L.Billinge^{2,3},
and Stanislaus S. Wong^{1,3*}

¹Department of Chemistry, State University of New York at Stony Brook,
Stony Brook, NY 11794-3400

²Department of Applied Physics and Applied Mathematics, Columbia University,
New York, NY 10027

³Condensed Matter of Physics and Materials Sciences Division,
Brookhaven National Laboratory, Upton, NY 11973

*To whom correspondence should be addressed.

Email: Stanislaus.wong@stonybrook.edu; sswong@bnl.gov

Phone: 631-632-1703; 631-344-3178

X-ray Diffraction – Experimental Protocol

The crystallographic purity of as-prepared Co-substituted NaFeSi₂O₆ NW bundles were confirmed using powder XRD. To prepare a typical sample for analysis, a fixed quantity of material was dispersed in ethanol and sonicated for ~1 min, prior to further air-drying upon deposition onto the sample holder. Diffraction patterns were subsequently obtained using a Rigaku Ultima III diffractometer, operating in the Bragg configuration using Cu K α radiation (1.54 Å) and as a function of varying 2 θ from 20 to 60° at a scanning rate of 1.0°/min for Co-based pyroxene bundles.

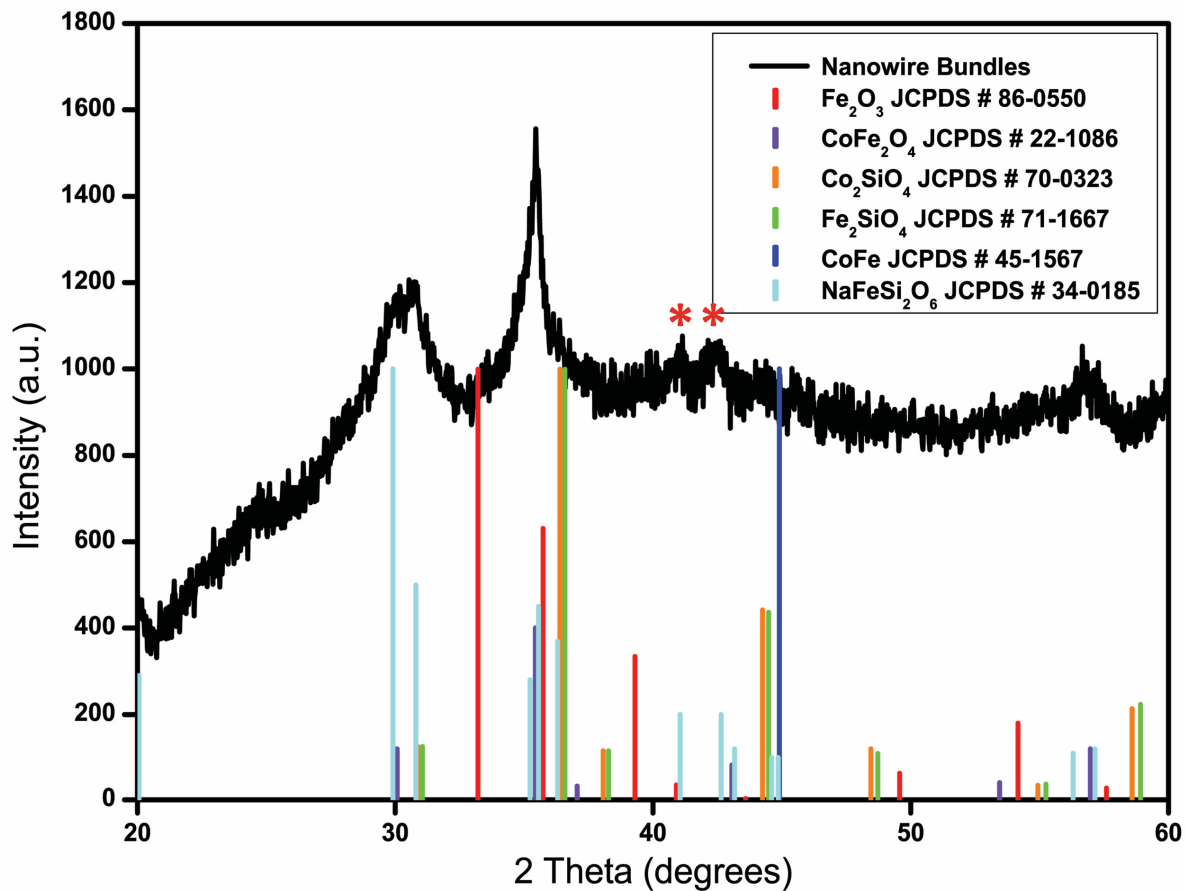


Figure S1. XRD pattern of as-prepared Co-substituted $\text{NaFeSi}_2\text{O}_6$ NW bundles, synthesized via a hydrothermal method, as compared with standards for a number of different model compounds. The red asterisks correspond to sodium silicate (Na_2SiO_3), as suggested by the database standard, JCPDS # 01-0836.

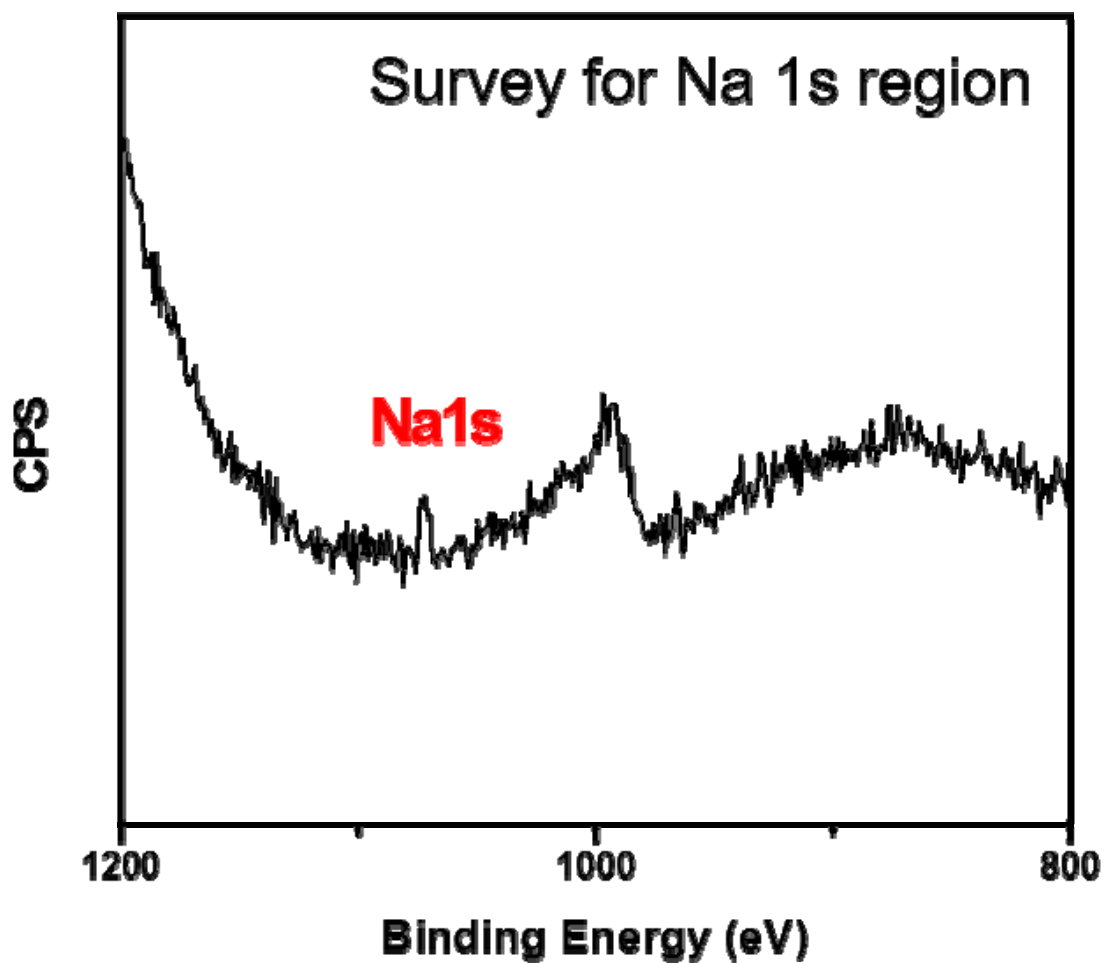


Figure S2. Magnified XPS survey spectrum with the Na *1s* region highlighted.

Table S1: Information for all structures tested against the PDF data is tabulated. The results of the Pearson correlation calculation between model and experimental PDFs are shown. The most highly correlated model results are highlighted (red > orange).

			Composition	Name	Space group	Pearson DM154_1
	Database	#				
1	AMCSD	0009492	Na Sc Si ₂ O ₆	Jervisite	C 1 2/c 1	0.67
2	COD	9000393	Co ₂ (Si O ₄)	Co-olivine	I m m a	0.19
3	COD	9005438	Na Fe Si ₂ O ₆	Aegirine	C 1 2/c 1	0.92
4	COD	9007046	Fe ₂ O ₄ Si	Fayalite	P n m a	0.23
5	ICSD	844	Fe ₂ (Si O ₄)	Spinel-Al ₂ MgO ₄	F d -3 m S	0.17
6	ICSD	845	Co ₂ (Si O ₄)	Spinel-Al ₂ MgO ₄	F d -3 m S	0.20
7	ICSD	4353	Fe ₂ Si O ₄	Olivine-Mg ₂ SiO ₄	P b n m	0.21
8	ICSD	4369	Na ₆ Fe (Al ₄ Si ₈ O ₂₆)	Naujakasite	C 1 2/m 1	-0.06
9	ICSD	6248	Co ₂ (Si O ₄)	Olivine-Mg ₂ SiO ₄	P b n m	0.23
10	ICSD	8132	Co ₂ Si O ₄	Mn ₂ GeO ₄	I m m a	0.19
11	ICSD	9362	Co ₃ O ₄	Spinel-Al ₂ MgO ₄ , reduced symmetry	F -4 3 m	0.19
12	ICSD	9671	Na Fe Si ₂ O ₆	Pyroxene-CaMg(SiO ₃) ₂	C 1 2/c 1	0.92
13	ICSD	10480	Li Al ₅ O ₈	Spinel-LiFeO ₈	P 43 3 2	-0.06
14	ICSD	15388	Na ₂ (Si O ₃)	Na ₂ SiO ₃	C m c 21	-0.15
15	ICSD	17054	Co (Si O ₃)	Pyroxene-MgSiO ₃ (cobaltian)	P b c a	0.68
16	ICSD	34669	Na ₂ (Si ₂ O ₅)	Li ₂ Si ₂ O ₅	P c n b	-0.02
17	ICSD	34688	Na ₂ (Si ₂ O ₅)	Na ₂ Si ₂ O ₅ (Natrrosilite)	P 1 21/a 1	-0.04
18	ICSD	34950	Na ₂ Li Fe Si ₆ O ₁₅	Tuhualite (Emeleusite)	A c a m	0.21
19	ICSD	41257	(Fe _{2.38} Co _{0.62} O ₄)	Spinel-Al ₂ MgO ₄	F d -3 m S	0.21
20	ICSD	62594	Na ₄ (Si O ₄)	Na ₄ SiO ₄	P -1	0.31
21	ICSD	64802	Fe _{1.58} (Si O ₄)	Laihunite 3M substructure	P 21/b 1 1	0.09
22	ICSD	66759	(Co Fe ₂) O ₄	CoFe ₂ O ₄	R -3 m H	0.21
23	ICSD	68984	Na (Fe O ₂)	NaFeO ₂ (beta)	P n 21 a	0.17
24	ICSD	68985	Na _{0.975} (Fe _{0.975} Si _{0.025}) O ₂	NaFeO ₂ (beta)	P n 21 a	0.24
25	ICSD	68986	Na _{0.95} (Fe _{0.95} Si _{0.05}) O ₂	NaFeO ₂ (beta)	P n 21 a	0.17
26	ICSD	68987	Na _{0.925} (Fe _{0.925} Si _{0.075}) O ₂	NaFeO ₂ (beta)	P n 21 a	0.17
27	ICSD	68988	Na _{0.9} (Fe _{0.9} Si _{0.1}) O ₂	NaFeO ₂ (beta)	P n 21 a	0.16
28	ICSD	68989	K (Ga O ₂)	KAlO ₂	P b c a	0.29
29	ICSD	68990	Na _{0.895} (Fe _{0.905} Si _{0.095}) O ₂	(NaFe) _{1-x} Si _x O ₂	P b c a	0.42
30	ICSD	74640	Na ₂ (Si O ₃)	Na ₂ SiO ₃	C m c 21	-0.13
31	ICSD	80378	Na ₂ (Si ₂ O ₅)	Epsilon sodium silicate	P b c 21	0.18
32	ICSD	81134	Na ₂ (Si ₃ O ₇)	Na ₂ Si ₃ O ₇ (mS48)	C 1 2/c 1	0.14
33	ICSD	82410	Na ₂ Si (Si ₃ O ₉)		P 1 21/n 1	0.25
34	ICSD	84819	Na ₂ Co (Si ₄ O ₁₀)	KNa ₂ FeS ₁₄ O ₁₀	P -1	0.41
35	ICSD	85551	Na ₈ Si (Si ₆ O ₁₈)		R -3 R	-0.04
36	ICSD	98551	(Co _{0.465} Fe _{0.535}) (Co _{1.535} Fe _{0.465}) O ₄	Spinel-Al ₂ MgO ₄	F d -3 m Z	0.22
37	ICSD	98564	Na ₂ (Si ₂ O ₅)	Na ₂ Si ₂ O ₅ (oP36)	P n 21 a	0.23
38	ICSD	98710	Na ₂ (Si ₂ O ₅)		I 41/a Z	-0.08
39	ICSD	109044	Co Fe ₂ O ₄	Spinel-Al ₂ MgO ₄	F d -3 m S	0.20
40	ICSD	154114	Na ₆ (Si ₈ O ₁₉)		P 1 21/c 1	0.08
41	ICSD	166645	Na _{0.628} ((Co _{0.97} Fe _{0.03}) O ₂)	NaxCoO ₂	P 63/m m c	-0.17
42	ICSD	200805	K ₂ Na ₂ Fe ₂ (Si ₄ O ₁₀) ₂	KNa ₂ FeS ₁₄ O ₁₀	P -1	0.02
43	ICSD	240870	K ₂ Na ₂ Fe ₂ (Si ₄ O ₁₀) ₂	KNa ₂ FeS ₁₄ O ₁₀	P -1	0.53
44	ICSD	250222	K ₂ Na ₂ Fe ₂ (Si ₄ O ₁₀) ₂	KNa ₂ FeS ₁₄ O ₁₀	P -1	0.21

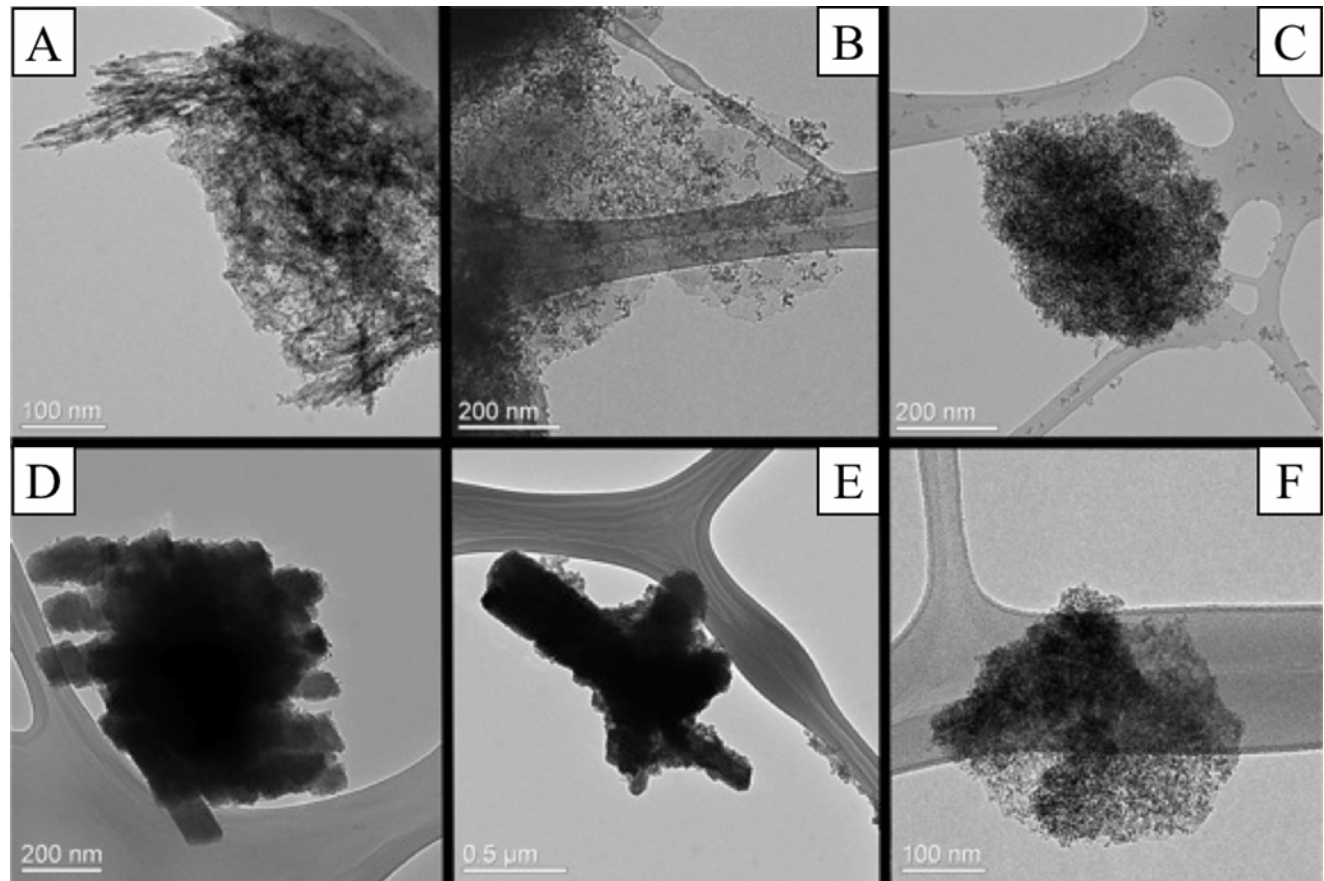


Figure S3. Control experiments associated with the synthesis of Co-substituted NaFeSi₂O₆ nanostructures in the absence of NaOH. Reactions were run either in (A-C) water or in (D-F) 1:1 volume ratios of H₂O/EtOH for 6, 12, and 24 hours, respectively.

Probing the role of bases toward nanowire growth

The idea of the key significance of the identity of the base (Figure S4) was duly studied for the Co-substituted NaFeSi₂O₆ system, by altering the base from NaOH to either KOH or NH₄OH, and subsequently systematically varying the metal cations from the bases used, i.e. NaOH, KOH, and NH₄OH, associated with Na⁺, K⁺, and NH₄⁺, respectively. All other reaction parameters were kept identical. Though NaOH and KOH are considered to be strong bases and hence completely dissociate, NH₄OH is a comparatively weaker base and has a finite dissociation constant.

We found that use of NaOH yields typical anisotropic structures (Figure S4A). By contrast, employing KOH gave rise to a very different morphology, i.e. nanoplates (Figure S4B). Interestingly, NH₄OH produced the ‘least regular’ nanoscale structures, and in fact, led to the generation of a complex morphologically inhomogeneous mixture, comprised of particles, sheets, and oriented motifs, as observed by TEM (Figure S4C).

We note that the morphologies observed when using NH₄OH resembled samples collected at early reaction times for other bases. Given these observations, it is plausible that unlike Na⁺ and K⁺, NH₄⁺ likely does not participate directly in inducing the formation of the resulting isolated morphology. Cations are understood to influence structure formation during mineralization and are known to induce the production of zeolites under classical hydrothermal conditions. However, they can also affect the stability of the colloidal suspension.¹⁻⁴ Specifically, structure-directing effects from cations can be inferred by varying the nature of the base from KOH to NaOH.⁵ These effects may be related to the physical sizes of the cationic radii, associated with the respective cations of the bases used. In particular, the radii of the ions are Na⁺ = ~1.149 Å, K⁺ = 1.97 Å, and NH₄⁺ = 2.107 Å, respectively.⁶ The importance of these ions in

controlling crystal structure growth has been previously analyzed for bismuth ferrite, BiFeO_3 .⁷ Specifically, this study highlighted the key role of MOH ‘mineralizers’ ($M = \text{K}^+$, Na^+ and Li^+) in determining the resulting ferrite crystal size and morphology observed. In effect, the proposed growth mechanisms for the use of each of these ‘mineralizers’ suggest a profound influence of these particular cations upon the crystallization process of BiFeO_3 , and therefore, accentuates the significance of the presence of Na^+ within our own specific systems herein.

To further reinforce this conclusion, the corresponding diffraction patterns (Figure S5) for samples derived from NaOH , KOH , and NH_4OH are indeed different and distinctive. Most compelling is the difference in patterns between the use of NaOH and KOH (Figure S5), wherein observed diffraction peaks are present at different locations. This result provides evidence that whether Na^+ or K^+ is utilized affects the net observed structure.

It should be further noted that we observed a diffuse diffraction pattern associated with the sample prepared using NH_4OH , which was similar to analogous data taken from samples generated using low reaction times, because it is likely that the polyatomic ion radius (i.e. $\text{NH}_4^+ = \sim 2.107 \text{ \AA}$) may be too large to stabilize nanowire formation. These observations might have resulted from either the ultra-small nanoscale dimensions of the as-prepared particles or the relatively low crystallinity from the resulting as-prepared sample.

Role of ionic species in growth mechanism

We have employed elemental mapping from energy dispersive x-ray (EDX) analysis to corroborate our growth mechanism. Specifically, a reduced reaction time, i.e. 1 hour, was used to generate ‘early-reaction’ products in order to establish the mechanistic roles of ionic species, such as anionic silicates and cationic sodium. The spatial relationships of elements (Figure S6)

highlight localization of all expected elements within our cobalt ferrite synthesis, i.e. O, Na, Si, Fe, and Co within our observed aggregated particles.

The spatial overlap between Si and Na is consistent with a degree of coordination between these ionic species associated with the precipitation of cobalt ferrites. Furthermore, we studied the elemental composition of the resulting 1D structures (Figure S7) in experiments both with and without the use of the cobalt precursor. What we noted is that in the absence of CoCl_2 , our Co-substituted $\text{NaFeSi}_2\text{O}_6$ products are comparable in morphology, specifically with regards to Si content. We consider the results of our ‘cobalt free’ synthesis to corroborate the importance of our silicate structures in the context of generating a 1D morphology. TEM images (Figure S9) highlight the formation of wire bundles grown in the absence of a cobalt precursor.

Furthermore, we studied the nature of structural features, specifically associated with that of the silicates, evolving as a function of the reaction time. Infrared spectroscopy (IR) was used to probe either the presence or absence of metal oxide bonds at different reaction times. Structurally, we posit the 1D alignment of silicate chains as the basis of our silicate-assisted growth mechanism, wherein we expect an underlying Si-O network comprising the structural framework or backbone for our anisotropic structures.

Spectra were collected at different reaction times, i.e. at 1 hour and at 5 hours, and our final product (Figure S8) highlighted the evolution of features, indicative of Si-O-Si network bonds. Specifically, we noted evidence for Si-OH, denoting the terminal deformation band⁸ located at around 950 cm^{-1} ; the 5-hour reaction sample contained additional features associated with Si-O-Si and O-Si-O bond stretching frequencies⁹ situated at around 1090 cm^{-1} . This feature persisted into the final wire-like products. Indeed, the evolution of this secondary stretching frequency is indicative of an underlying silicate network within our final anisotropic structure.

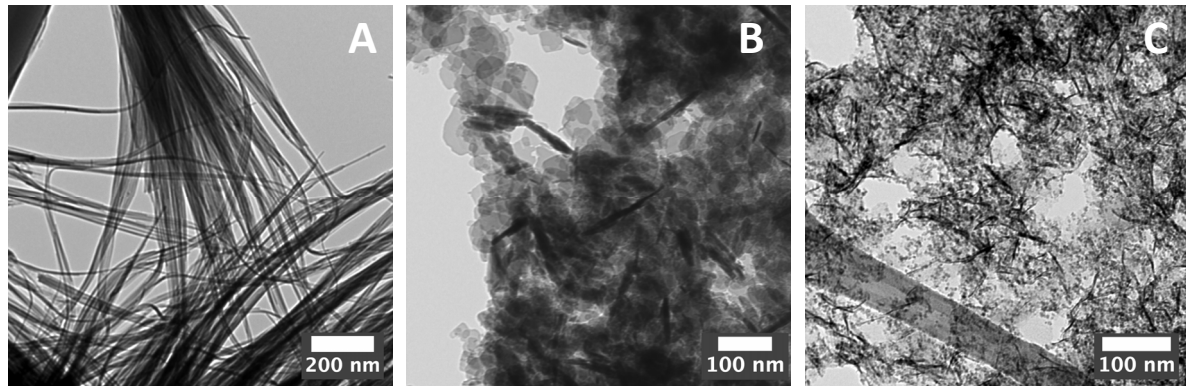


Figure S4. TEM images for control experiments associated with the synthesis of Co-substituted $\text{NaFeSi}_2\text{O}_6$ nanostructures in the presence of various bases, such as (A) NaOH , (B) KOH , and (C) NH_4OH , respectively.

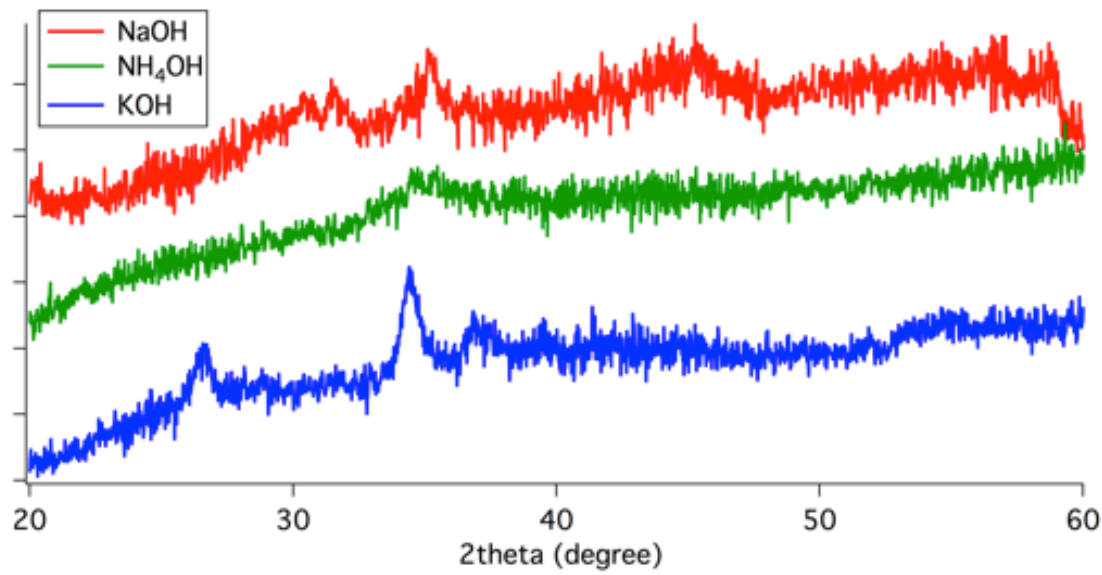


Figure S5. XRD patterns for control experiments associated with the synthesis of Co-substituted $\text{NaFeSi}_2\text{O}_6$ nanostructures in the presence of various bases, including NaOH (red), NH_4OH (green), and KOH (blue), respectively.

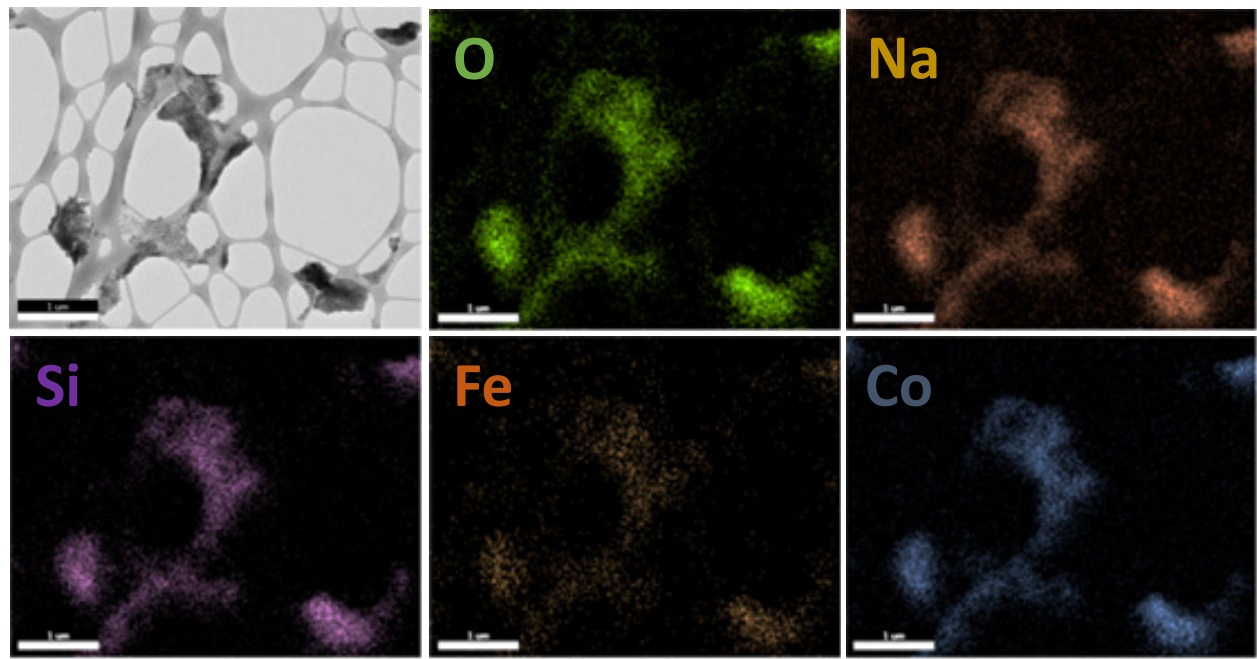


Figure S6. Elemental mapping for structures generated after 1 hour of reaction time. STEM image and respective elemental maps for O, Na, Si, Fe, and Co are presented. Scale bar is 1 μ m.

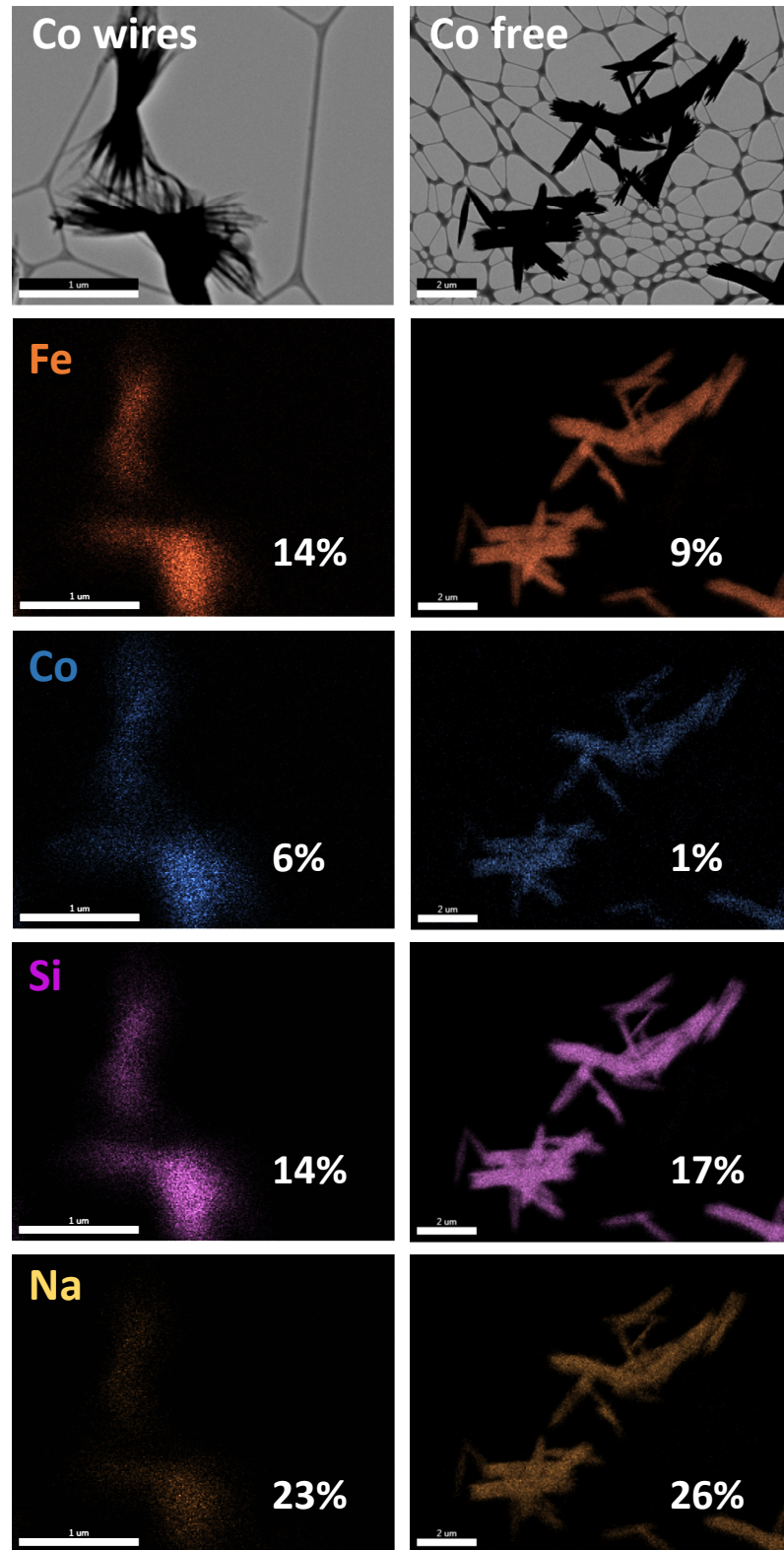


Figure S7. Elemental mapping images for typical Co-substituted $\text{NaFeSi}_2\text{O}_6$ wires (left) and cobalt-free analogue (right). STEM image and respective elemental maps for Fe, Co, Si, and Na. Atomic percents for the various metallic elements are shown. Scale bar is $1 \mu\text{m}$.

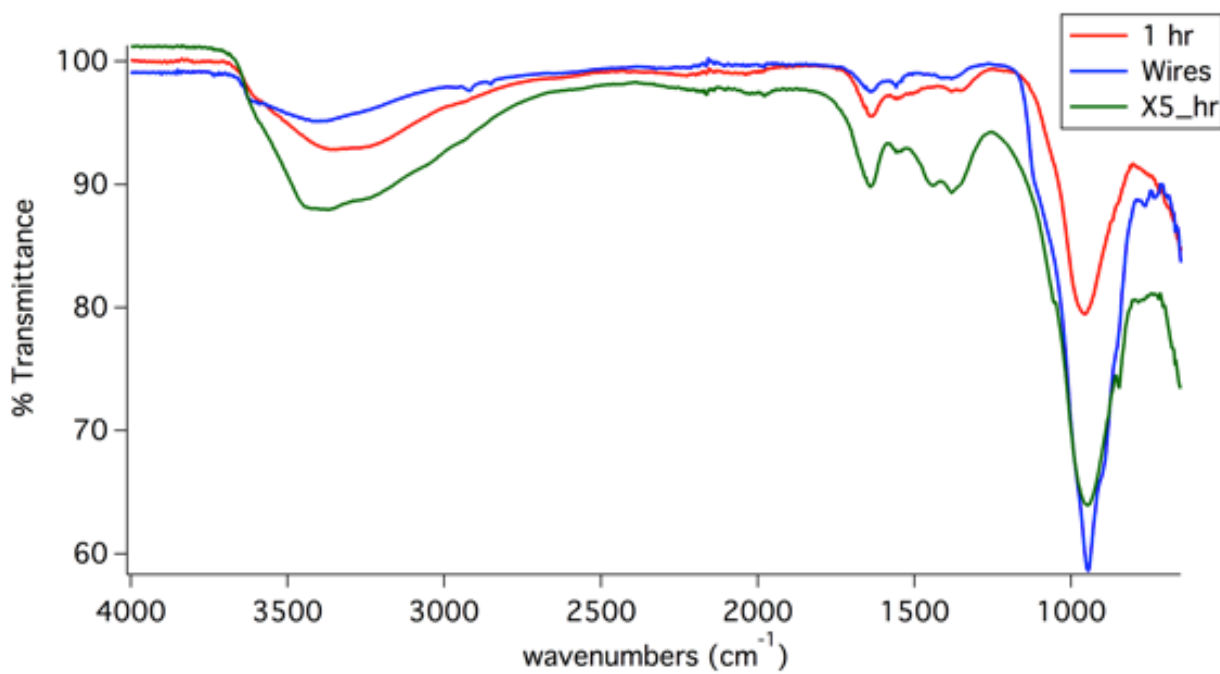


Figure S8. Infrared spectra for samples prepared after 1 hour of reaction time (red) and 5 hours of reaction time (green), respectively. Data for the resulting wires (blue), obtained at reaction completion, are also presented.

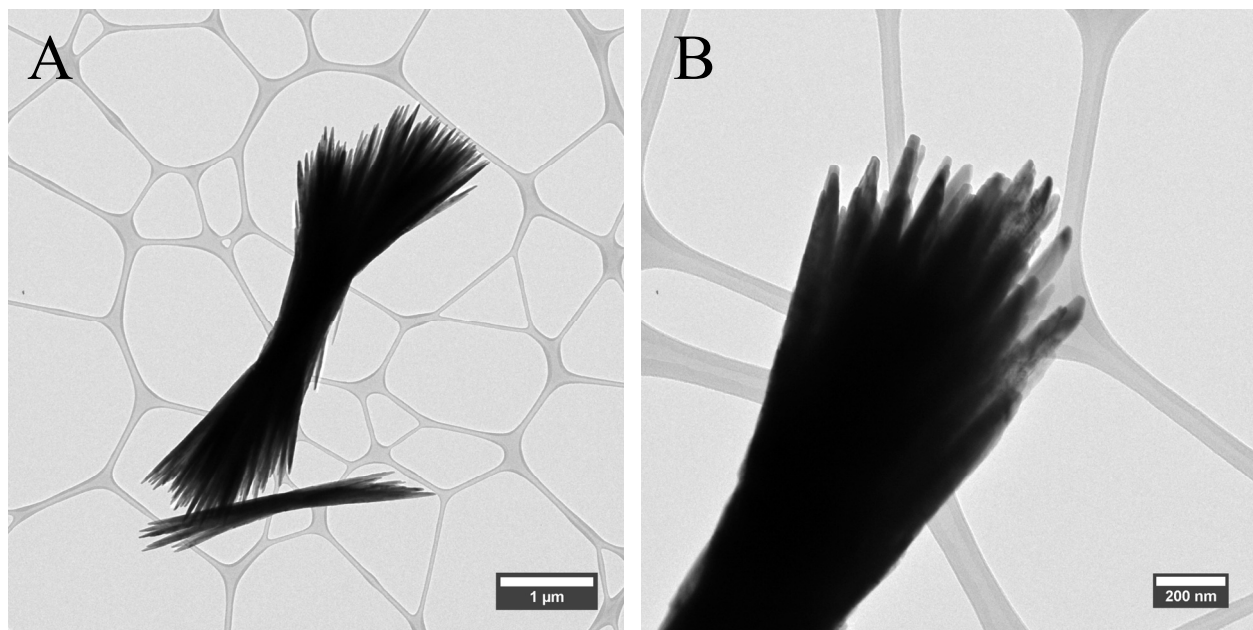


Figure S9. TEM images derived from a ‘cobalt-free’ synthesis wherein bundle motifs are observed at lower magnification (A). Wire-like motifs are noted at higher magnification (B) with distinctive average diameters ranging from 30 to 40 nm.

References

1. R. M. Barrer, *Zeolites*, 1981, **1**, 130-140.
2. M. R. Johan, N. A. K. Aznan, S. T. Yee, I. H. Ho, S. W. Ooi, N. D. Singho and F. Aplop, *Journal of Nanomaterials*, 2014, 1-7.
3. Z. Wang, J.-G. Li, Q. Zhu, B.-N. Kim and X. Sun, *Materials & Design*, 2017, **126**, 115-122.
4. L. R. Tsuruta and A. M. Carmona-Ribeiro, *The Journal of Physical Chemistry*, 1996, **100**, 7130-7134.
5. R. A. Rakoczy, M. Breuninger, M. Hunger, Y. Traa and J. Weitkamp, *Chemical Engineering and Technology*, 2005, **25**, 273-275.
6. P. F. Lang and B. C. Smith, *Dalton Trans*, 2010, **39**, 7786-7791.
7. H. Mirabbos, X. Yunhua, W. Fazhan, W. Juan, L. Wengang and W. Mingqiong, *Ceramics - Silikaty*, 2009, **53**, 113-117.
8. M. G. Fonseca, A. S. Oliveira and C. Airoldi, *Journal of Colloid and Interface Science*, 2001, **240**, 533-538.
9. R. A. Nyquist and R. O. Kagel, *Infrared Spectra of Inorganic Compounds*, Academic, New York, 1971.